CHIN. PHYS. LETT. Vol. 38, No. 5 (2021) 057301

Magnus Hall Effect in Two-Dimensional Materials

Rui-Chun Xiao(肖瑞春)[1,2,3], Zibo Wang(王孜博)[4,5], Zhi-Qiang Zhang(张智强)[2], Junwei Liu(刘军伟)[6*], and Hua Jiang(江华)[2,3*]

[1]*Institute of Physical Science and Information Technology, Anhui University, Hefei 230601, China*
[2]*School of Physical Science and Technology, Soochow University, Suzhou 215006, China*
[3]*Institute for Advanced Study, Soochow University, Suzhou 215006, China*
[4]*College of Physics and Electronic Engineering, Sichuan Normal University, Chengdu 610068, China*
[5]*Center for Computational Sciences, Sichuan Normal University, Chengdu 610068, China*
[6]*Department of Physics, Hong Kong University of Science and Technology, Clear Water Bay, Hong Kong, China*

(Received 11 January 2021; accepted 25 February 2021; published online 2 May 2021)

The Magnus Hall effect (MHE) is a new type of linear-response Hall effect, recently proposed to appear in two-dimensional (2D) nonmagnetic systems at zero magnetic field in the ballistic limit. The MHE arises from a self-rotating Bloch electron moving under a gradient-electrostatic potential, analogous to the Magnus effect in the macrocosm. Unfortunately, the MHE is usually accompanied by a trivial transverse signal, which hinders its experimental observation. We systematically investigate the material realization and experimental measurement of the MHE, based on symmetry analysis and first-principles calculations. It is found that both the out-of-plane mirror and in-plane two-fold symmetries can neutralize the trivial transverse signal to generate clean MHE signals. We choose two representative 2D materials, monolayer MoS_2, and bilayer WTe_2, to study the quantitative dependency of MHE signals on the direction of the electric field. The results are qualitatively consistent with the symmetry analysis, and suggest that an observable MHE signal requires giant Berry curvatures. Our results provide detailed guidance for the future experimental exploration of MHE.

DOI: 10.1088/0256-307X/38/5/057301

Following decades of extensive studies, it has now been demonstrated that the intrinsic anomalous Hall effect[1] originates from nonzero Berry curvature, which can be viewed as a pseudo-magnetic field.[2] An electron wave packet with nonzero Berry curvature moving through an electric field will acquire an additional shift, perpendicular to the electric field.[3,4] It is easy to prove that the total Berry curvature is zero, and that the Hall conductivity vanishes in a time-reversal symmetric system; it can even emerge locally in momentum space.[5] For some time, therefore, the majority of studies concerning Berry curvature have focused on magnetic systems.[1,2,6,7] Recently, however, various Hall effects in time-reversal symmetric systems, such as the nonlinear Hall effect[8–12] and the gyrotropic Hall effect,[13–15] have been proposed and experimentally verified. These have stimulated great interest in the discovery of additional Hall effects in non-magnetic materials.

Very recently, Papaj and Fu proposed a new type of Hall effect, analogous to the Magnus effect in the macrocosm, known as the Magnus Hall effect (MHE),[16] where even the nonzero local Berry curvature in time-reversal symmetric systems can give rise to a linear-response Hall effect in the ballistic limit. Based on the ideal model analysis, the MHE is predicted to offer a way to measure the distribution of the Berry curvature on the Fermi surface.[16] However, the material realization of MHE is yet to be achieved, as experiments must be performed using suitable materials. Therefore, the determination of 2D materials exhibiting the MHE is key. However, a trivial transverse current may accompany the MHE signal in general, which may disturb the experimental observation. Consequently, how to eliminate its effect on materials under experimental conditions also needs to be clarified. Finding suitable material candidates exhibiting the MHE, and studying their responses under feasible and realistic conditions is critical to the success of future experimental studies.

In this Letter, we study the symmetry requirements for the realization of a clean MHE, and numerically calculate the dependence of MHE conductance and trivial transverse conductance for real materials, based on first-principles calculations. We find that the trivial transverse signals are very large in general. Nevertheless, out-of-plane mirror and in-plane two-fold symmetries can effectively eliminate the trans-

Supported by the National Basic Research Program of China (Grant No. 2019YFA0308403), the National Natural Science Foundation of China (Grant Nos. 11822407, 11947212, 11704348, and NSFC20SC07), the China Postdoctoral Science Foundation (Grant No. 2018M640513), and the Hong Kong Research Grants Council (Grant Nos. 26302118, 16305019, and N_HKUST626/18).
*Corresponding author. Email: liuj@ust.hk; jianghuaphy@suda.edu.cn
© 2021 Chinese Physical Society and IOP Publishing Ltd

verse signa. We find that 2D materials with giant Berry curvature make it easier to observe the MHE signal.

Symmetry Analysis. In MHEs, a Hall bar device, composed of a 2D material, is placed on the bottom gate, where the source and drain regions have different local bottom gate voltages, leading to a gradient-electrostatic potential, $\partial U/\partial x$, along the longitudinal (x) direction. The Berry curvature $\Omega(\boldsymbol{k})$ only has a z component in 2D systems, i.e., $\Omega_z(\boldsymbol{k})$. If the system exhibits nonzero local Berry curvature $\Omega_z(\boldsymbol{k})$, the propagating electrons can obtain an anomalous transverse (y) velocity proportional to $\Omega_z(\boldsymbol{k})(\partial U/\partial x)$. A small bias voltage $V_{\rm sd}$ is then applied between the source and the drain. In this way, electrons with positive velocity v_x are injected into the system, and propagate without any scattering in the ballistic limit.[16] The anomalous transverse velocity leads to an additional MHE current. In this case, the transverse charge current density is[16]

$$j_y = j_y^0 + j_{\rm H}, \tag{1}$$

where

$$j_y^0 = -\frac{e\Delta\bar{\mu}}{(2\pi)^2}\sum_n \int_{v_{n,x}(\boldsymbol{k})>0} v_{n,y}(\boldsymbol{k})\Big(-\frac{\partial f_n(\boldsymbol{k})}{\partial \epsilon_n(\boldsymbol{k})}\Big)d^2\boldsymbol{k}, \tag{2}$$

and

$$j_{\rm H} = \frac{e}{h}\frac{\Delta\bar{\mu}}{2\pi}\sum_n \int_{v_{n,x}(\boldsymbol{k})>0} \Omega_{n,z}(\boldsymbol{k})\frac{\partial U}{\partial x}\Big(-\frac{\partial f_n(\boldsymbol{k})}{\partial \epsilon_n(\boldsymbol{k})}\Big)d^2\boldsymbol{k}. \tag{3}$$

Here, $\Delta\bar{\mu} = eV_{\rm sd}$, and $v_{n,a}(\boldsymbol{k}) = (1/\hbar)\partial\epsilon_n(\boldsymbol{k})/\partial k_a$ [$a \in \{x, y\}$, where n is the band index] is the electron velocity. In Eq. (2), j_y^0 stands for the trivial transverse current density, which arises from the transverse velocity anisotropy of the Fermi surface. In Eq. (3), $j_{\rm H}$ represents the MHE current density. The factor $\partial f_n(\boldsymbol{k})/\partial\epsilon_n(\boldsymbol{k})$ in Eq. (3) implies that the MHE current is a Fermi surface-determined quantity. Even though the sum of $\Omega_{n,z}(\boldsymbol{k})$ across the whole Brillouin zone is zero under time-reversal symmetry, the sum of $\Omega_{n,z}(\boldsymbol{k})$ with positive v_x [Eq. (3)] can be nonzero. Therefore, the MHE current $j_{\rm H}$ can emerge in time-reversal materials.

Firstly, we identify those symmetries hosting nonzero Berry curvature in 2D materials. Under inversion symmetry $\mathcal{I}$, $\Omega_{n,z}(\boldsymbol{k}) = \Omega_{n,z}(-\boldsymbol{k})$. Moreover, $\Omega_{n,z}(\boldsymbol{k})$ is odd under time-reversal symmetry $\mathcal{T}$, $\Omega_{n,z}(\boldsymbol{k}) = -\Omega_{n,z}(-\boldsymbol{k})$. Therefore, $\Omega_{n,z}(\boldsymbol{k})$ is zero under both $\mathcal{T}$ and $\mathcal{I}$ symmetries. Following the above guidelines, eleven crystallographic point groups exhibiting inversion symmetry are excluded. In addition, three non-centrosymmetric cubic point groups, $T(23)$, $O(432)$, and $T_h(\bar{4}3\,m)$, are also excluded, as they cannot exist in 2D materials. In a 2D system, $\mathcal{C}_{2z}$ gives rise to $\boldsymbol{k} \to -\boldsymbol{k}$ as the inversion symmetry $\mathcal{I}$, such that materials with $\mathcal{C}_{2z}$ and $\mathcal{T}$ also have zero local Berry curvature. Therefore, point groups containing $\mathcal{C}_{2z}$, $\mathcal{C}_{4z}$, $\mathcal{S}_{4z}$, and $\mathcal{C}_{6z}$ symmetry operations also force the Berry curvature to zero, since these operations all include $\mathcal{C}_{2z}$ symmetry. Given the above considerations, the point groups allowing nonzero local Berry curvature in 2D systems are $C_1(1)$, $C_{1h}(m)$, $C_{1v}(m)$, $C_2(2)$, $C_{2v}(2mm)$, $C_3(3)$, $C_{3h}(\bar{6})$, $C_{3v}(3m)$, $D_3(32)$, and $D_{3h}(\bar{6}m2)$. In the C_{2v} and C_2 groups, the $\mathcal{C}_2$ symmetry operation is in the 2D plane, rather than vertical to the plane ($\mathcal{C}_{2z}$). Of these, $D_{3h}(\bar{6}m2)$ has the highest symmetry, and the other 9 point groups constitute its subgroups.

Moreover, the nonzero j_y^0 in Eq. (2) interferes with any observation of the MHE under experimental conditions. We should therefore find symmetries to eliminate this. Firstly, we consider the vertical mirror $\mathcal{M}$ symmetry. Basically, there are two choices in terms of the placement of vertical mirror $\mathcal{M}$ symmetry: parallel ($\mathcal{M}_{xz}$) or perpendicular ($\mathcal{M}_{yz}$) to the direction of driving current (x), as illustrated in Fig. 1. Under the $\mathcal{M}_{yz}$ and time-reversal symmetry, $\mathcal{T}$, one $\boldsymbol{k}$ point will transfer into four. The relationships of both Fermi velocity and Berry curvature with these four points are shown in Fig. 1(a). If we assume $v_x > 0$, the points that contribute to the transverse current are $\mathcal{E}\boldsymbol{k}$ (where $\mathcal{E}$ refers to the identity symmetry) and $\mathcal{T}\cdot\mathcal{M}_{yz}\boldsymbol{k}$. Note that j_y^0 is zero, while $j_{\rm H}$ is non-zero, according to Eqs. (2) and (3). In contrast, $\mathcal{M}_{xz}$ forces both j_y^0 and $j_{\rm H}$ to be zero, given that $\boldsymbol{k}$ points with positive v_x have both opposite v_y and Ω_z, as plotted in Fig. 1(b). The in-plane $\mathcal{C}_2$ symmetry produces the same effects as vertical mirror $\mathcal{M}$ symmetry. For example, under $\mathcal{C}_{2x}$ or $\mathcal{M}_{xz}$ symmetry: $k_x \to k_x$, $k_y \to -k_y$, in the meantime $v_x \to v_x$, $v_y \to -v_y$, and $\Omega_{n,z} \to -\Omega_{n,z}$. Therefore, j_y^0 will be neutralized under the $\mathcal{C}_{2x}$ symmetry.

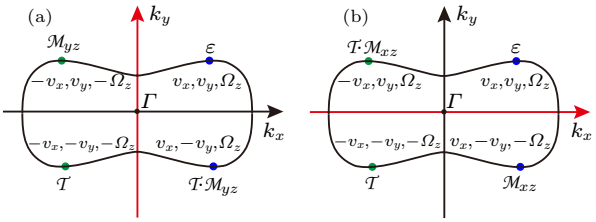

Fig. 1. Schematic diagram for symmetry of the Berry curvature and velocity of under (a) $\mathcal{M}_{yz}$ and (b) $\mathcal{M}_{xz}$. The red axis means where the mirror operation locates. If $v_x > 0$, the $\boldsymbol{k}$ points with positive and negative v_x are colored by blue and green, respectively. $\mathcal{E}$ means the identity operator.

On the other hand, horizontal mirror $\mathcal{M}_{xy}$ symmetry places no constraint on the Berry curvature and velocity, and $\mathcal{C}_{3z}$ rotation symmetry cannot guarantee the vanishing of j_y^0 (see the Supplement Materials)

either.[17] Therefore, j_y^0 cannot be neutralized by the C_1, C_{1h}, C_3, and C_{3h} point groups.

Based on the above analysis, we summarize the symmetries permitting MHE, and plot them in Fig. 2. For the point groups in the red area, j_y^0 can be eliminated when the $\mathcal{C}_2$ or the $\mathcal{M}$ symmetry is perpendicular to the x axis (i.e., the driving current direction), and one can obtain a clean MHE signal. Based on the symmetry analysis above, we go through the 2D materials database[18−20] to screen for materials satisfying the symmetries given in Fig. 2, and list some representative candidate materials in Table 1. Most of the materials in the table with symmetries falling within the red area of Fig. 2 have been experimentally synthesized. The majority of these belong to the transition metal dichalcogenide, e.g., MoS_2, WTe_2, and TaS_2. Some of them are metals (e.g., TaS_2, and NbS_2) and some are semiconductors (e.g., MoS_2, GaSe, and In_2Se_3). Most of the materials whose symmetries fall within the blue area of Fig. 2 are theoretically predicted.[18−20] Specifically, these materials contain heavy elements with strong spin-orbit coupling effects, and larger Berry curvatures can be expected. Since the MHE is a property of the Fermi surface, the semiconductors should be gated to metals, which provide easy access for 2D materials. Materials beyond Table 1, which are theoretically predicted, but have the potential to be synthesized experimentally, can also be selected, by virtue of the guidelines given in Fig. 2.

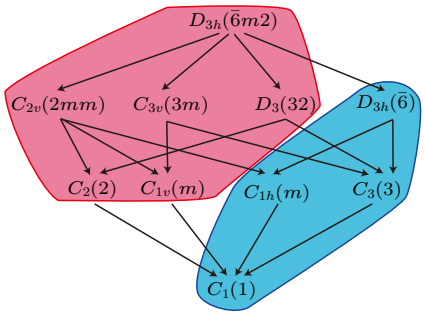

Fig. 2. Point groups permitting MHE. Here, C_{1v} indicates the presence of a vertical mirror ($\mathcal{M}_{xz}$ or $\mathcal{M}_{yz}$), perpendicular to the 2D plane. In C_{1h}, the horizontal mirror is located in the 2D plane, i.e., $\mathcal{M}_{xy}$. In C_2 and C_{2v}, the twofold symmetry, $\mathcal{C}_2$, lies in the 2D plane. The red area means that j_y^0 can be neutralized by symmetry, while the point groups in blue cannot eliminate j_y^0.

Table 1. Representative candidate 2D materials suitable for hosting MHE. The second column lists the corresponding layer groups. Most of these are taken from the 2D materials database,[18−20] with the exception of those with references.

Point group	Layer group	Material
D_{3h} ($\bar{6}m2$)	$p\bar{6}m2$, $p\bar{6}2m$	MoS_2, $MoSe_2$, WS_2, WSe_2 NbS_2, $NbSe_2$, TaS_2, $TaSe_2$, $ReSe_2$, GaS, GaSe, InSe, ZrSe, monolayer Na_3Bi,[21] In_2Se_3, $MoSi_2N_4$[22]
D_3 (32)	$p312$, $p321$	Ag_2Br_6, Bi_2I_6, Nb_2I_6, $AgIn_2PSe_6$
$C_{3v}(3m)$	$p31m$, $p3m1$	MoSSe,[23,24] TaSSe, TaSeTe, buckled GaAs (insulator),[25] Oxygen functionalized MXene,[26] Bismuthene on a SiC substrate[27]
C_{3h}	$p\bar{6}$	
$C_3(3)$	$p3$	Ir_2B_6, Cu_2Cl_6, ScP_2Se_6, $BiCuP_2Se_6$, $AgBiP_2Se_6$
$C_{2v}(2mm)$	$pm2m$, $pm2_1b$, $pb2_1m$, $pb2b$, $pm2a$, $pm2_1n$, $pb2_1a$, $pb2n$, $cm2m$, $cm2e$	Monolayer SnTe,[28] Uniaxial strained MoS_2[15]
$C_{1v}(m)$	$pm11$, $pb11$, $cm11$	Bilayer WTe_2,[9,10] bilayer $MoTe_2$, Monolayer WTe_2 under electric field,[11] Pb_2S_2
$C_2(2)$	$p211$, $p2_111$, $c211$	$ZrTeSe_4$, $ZrTeTe_4$
$C_{1h}(m)$	$p11m$, $p11a$	$Zr_4I_4S_4$, Mo_3WSe_8, $CrMo_3S_8$
C_1	$p1$	$AgNO_2$, Zr_2BSe_2, Pt_2Se_6, $Bi_2P_2S_6$, In_2Te_4

Calculation Methods. Based on the descriptions above, we obtain the permitted symmetry and candidate materials to host MHE. However, its magnitude requires further investigation. Here, we choose two representative 2D materials, monolayer MoS_2, and bilayer WTe_2, to perform our first-principles calcula-

tions (see the Supplemental Materials).[17] Whether or not the vertical mirror and in-plane two-fold symmetries can eliminate the trivial transverse signal j_y^0 in materials must be numerically verified. Moreover, in realistic experiments, the driving current may not be strictly perpendicular to these two symmetries. In addition, the angle-dependence measurement is an important experimental technique in material property characterization, e.g., the nonlinear Hall effect.[9] We should therefore study the angle-dependence of the MHE signal numerically. In the rotated coordinate, the band energy and Berry curvature are invariant, while the velocities of the electron are changed,

$$\begin{cases} v_x{}' = v_x \cos\theta + v_y \sin\theta, \\ v_y{}' = -v_x \sin\theta + v_y \cos\theta, \end{cases} \tag{4}$$

where θ indicates the rotation angle.

For convenience in comparing these two signals, we integrate the transverse current density, j_y^0 and $j_{\rm H}$, over the entire length of the device, and obtain the corresponding conductance. According to Eq. (3), the MHE conductance[16] is

$$G_{\rm H} = \frac{e^2}{h}\frac{\Delta U}{2\pi}\sum_n \int_{v_x(\boldsymbol{k})>0} \Omega_{n,z}(\boldsymbol{k})\Big(-\frac{\partial f_n(\boldsymbol{k})}{\partial \epsilon_n(\boldsymbol{k})}\Big) d^2\boldsymbol{k}, \tag{5}$$

where ΔU is the potential difference of the bottom gate. The trivial transverse conductance resulting from j_y^0 in Eq. (2) is

$$G_y^0 = -\frac{e^2}{h}\frac{L}{2\pi}\sum_n \int_{v_x(\boldsymbol{k})>0} \frac{\partial \epsilon_n}{\partial k_y}\Big(-\frac{\partial f_n(\boldsymbol{k})}{\partial \epsilon_n(\boldsymbol{k})}\Big) d^2\boldsymbol{k}, \tag{6}$$

where L denotes the length of the bottom gate.

Calculation Results. Monolayer MoS_2 is one of the most widely investigated 2D materials. It has a sandwich structure, with a $p\bar{6}m2$ layer group. According to Eq. (5), MHE conductance is zero when the chemical potential is inside the bandgap. As such, electron doping or gating is required to ensure a finite Fermi surface. The angle-dependence of the G_y^0 and $G_{\rm H}$ of MoS_2 are plotted in Fig. 3(a). We note that G_y^0 and $G_{\rm H}$ increase with chemical potential μ. Monolayer MoS_2 has three vertical mirror symmetries, at angles of 60° with one another. When the vertical mirror $\mathcal{M}$ symmetry is not perpendicular or parallel to the direction of the applied bias (i.e., $\theta \neq 30°n$, n is an integer), G_y^0 will emerge [see the upper panel in Fig. 3(a)]. Here, $G_{\rm H}$ becomes zero every 60° [see the lower panel in Fig. 3(a)]. The angle-dependence of $G_{\rm H}$ and G_y^0 are consistent with the symmetry analysis above. The ratio of $|G_{\rm H}/G_y^0|$ versus θ is plotted in Fig. 3(b). Here, $|G_{\rm H}/G_y^0|$ is at its maximum when the vertical mirror's $\mathcal{M}$ symmetry is perpendicular to the x direction, then decays quickly to nearly zero. That is to say, in order to observe the MHE, the vertical $\mathcal{M}$ plane should be strictly perpendicular to the driving current's (x) direction under experimental conditions.

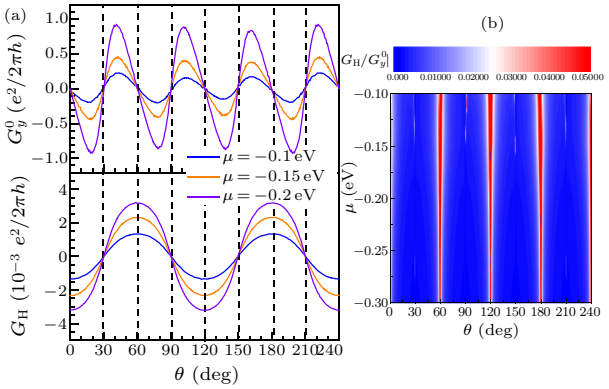

Fig. 3. Angle dependences of (a) $G_{\rm H}$ and G_y^0 of MoS_2 with variations in the chemical potential, μ. (b) Contour plot of $|G_{\rm H}/G_y^0|$ with different θ and μ angles. Here, $\Delta U = 0.2$ eV and $L = 50$ nm.

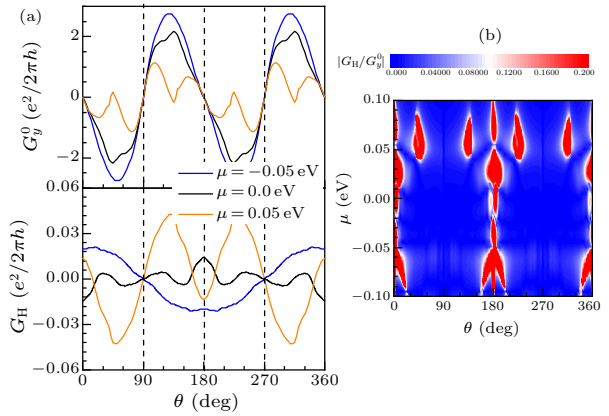

Fig. 4. (a) Angle dependences of $G_{\rm H}$ and G_y^0 of bilayer WTe_2. Here, $\Delta U = 0.1$ eV, and $L = 100$ Å, as given in Eq. (5). (b) $G_{\rm H}/G_y^0$ with different angles and chemical potentials. Here, $\Delta U = 0.1$ eV and $L = 100$ nm. The metallic ground state is obtained via our calculations.

Monolayer WTe_2 is a 2D topological insulator[29–31] with inversion symmetry, which prohibits the MHE. In bilayer WTe_2, the inversion symmetry $\mathcal{I}$ is broken due to the interlayer arrangement, and only the vertical mirror symmetry $\mathcal{M}$ survives ($\mathcal{M}_{yz}$).[9,10] The angle θ dependencies of both $G_{\rm H}$ and G_y^0 in bilayer WTe_2 are shown in Fig. 4(a). Here, G_y^0 is zero when the driving current is parallel or perpendicular to $\mathcal{M}_{yz}$ [see the upper panel in Fig. 4(a)], while $G_{\rm H}$ is zero only when the current is parallel to the mirror symmetry [see the lower panel in Fig. 4(a)]. The angle-dependence of $G_{\rm H}$ and G_y^0 are also consistent with the symmetry analysis given above. The ratio for $|G_{\rm H}/G_y^0|$ with various combinations of μ and θ is shown in Fig. 4(b), where the angle permitting the observation of sizeable MHE in WTe_2 is larger than that for MoS_2. The Berry curvature near the valence band maximum of monolayer MoS_2 is on the order of 10 Å^2,[32] the typical value for materials with the same

bandgaps. However, the corresponding Berry curvature of bilayer WTe_2 is on the order of 200 Å^2,[10] about 20 times larger than that of monolayer MoS_2. Therefore, the G_H in bilayer WTe_2 is much larger, and the angle permitting observation of the MHE is wider than that found in monolayer MoS_2. The comparison of these two materials suggests to us that both specific symmetry and a larger Berry curvature are required for observable MHE. Otherwise, the vertical $\mathcal{M}$ plane should be strictly perpendicular to the x direction in real-life experiments. Moreover, bilayer WTe_2 permits the nonlinear Hall effect,[9–11] which doubles the frequency of the AC driving current. It is therefore very easy to separate the nonlinear Hall effect from the MHE signal in the AC situation.

Furthermore, when both the driving bias, $\Delta\bar{\mu}$, and bottom gates, $\partial U/\partial x$, are reversed, the free carriers participating in the MHE are those where $v_x < 0$. If we assume that the $\boldsymbol{k}$ point with $v_x > 0$ contributes to the transverse current, its time-reversal, $\boldsymbol{k}$ with $v_x < 0$, will participate in the reverse situation. In accordance with Eqs. (2) and (3), j_y^0 remains invariant, while j_H will be reversed, because the Berry curvatures are opposite. Therefore, the total transverse current density changes from $j_y^0 + j_H$ to $j_y^0 - j_H$. The antisymmetric component of the total transverse current corresponds to the MHE current. The calculated G_H and G_y^0 of monolayer MoS_2 and bilayer WTe_2 do indeed exhibit this feature, as shown in Figs. 3(a) and 4(a). The antisymmetric characteristic is also verified by the nonequilibrium Green's function method (see the Supplemental Materials).[17] Therefore, reversing the current and bottom gates is an effective method for separating the two kinds of signals in real-life experiments, because it is easily accomplished. In addition, according to Eqs. (5) and (6), G_H linearly depends on ΔU, while G_y^0 does not. Therefore, the MHE signal can be separated by varying ΔU. This feature may be utilized experimentally to determine the MHE for small θ cases.

Discussions and Conclusion. Our MHE results have been obtained in the ballistic limit, with all the device lengths, L, adopted in the calculation above, below the typical mean-free paths, ξ, of these materials.[33,34] The finite relaxation time due to disorder will weaken, but not immediately destroy, the MHE, as long as the L is shorter than ξ.[16] It is therefore easier to measure the MHE in clean samples. The devices transmit from ballistic to diffusive transport when L is serval times larger than ξ,[35] where the MHE is proportional to the relaxation time, and has a similar form to the nonlinear Hall effect.[8]

In summary, we have identified the symmetry requirements (Fig. 2) for hosting MHE, and predicted its realization in various 2D materials (Table 1). When the direction of the driving current is perpendicular to the out-of-plane mirror, or the in-plane two-fold symmetry, the trivial transverse signal is zero, guaranteeing clean MHE signals. We have also performed a quantitative calculation of two representative materials, monolayer MoS_2 and bilayer WTe_2, based on first-principles calculations, and the results are consistent with our symmetry analysis. We also find that an observable MHE requires a large Berry curvature. Moreover, when the driving bias and gradient-electrostatic potential are reversed, the MHE conductance, G_H, inverts, while the trivial transverse conductance, G_y^0, is invariant, which can be utilized to separate the two kinds of signal under experimental conditions. Our work should prove instructive for the future determination of MHE materials, and the study of related properties in future experiments.

References

[1] Nagaosa N, Sinova J, Onoda S, MacDonald A H and Ong N P 2010 *Rev. Mod. Phys.* **82** 1539
[2] Fang Z, Nagaosa N, Takahashi K S, Asamitsu A, Mathieu R, Ogasawara T, Yamada H, Kawasaki M, Tokura Y and Terakura K 2003 *Science* **302** 92
[3] Chang M C and Niu Q 1995 *Phys. Rev. Lett.* **75** 1348
[4] Chang M C and Niu Q 1996 *Phys. Rev. B* **53** 7010
[5] Udagawa M and Bergholtz E J 2016 *Phys. Rev. Lett.* **117** 086401
[6] Li S, Lu J, Wen L J, Pan D, Wang H L, Wei D H and Zhao J H 2020 *Chin. Phys. Lett.* **37** 077303
[7] Shi G, Zhang M, Yan D, Feng H, Yang M, Shi Y and Li Y 2020 *Chin. Phys. Lett.* **37** 047301
[8] Sodemann I and Fu L 2015 *Phys. Rev. Lett.* **115** 216806
[9] Kang K, Li T, Sohn E, Shan J and Mak K F 2019 *Nat. Mater.* **18** 324
[10] Ma Q, Xu S Y, Shen H, MacNeill D, Fatemi V, Chang T R, Mier V A M, Wu S, Du Z, Hsu C H, Fang S, Gibson Q D, Watanabe K, Taniguchi T, Cava R J, Kaxiras E, Lu H Z, Lin H, Fu L, Gedik N and Jarillo-Herrero P 2019 *Nature* **565** 337
[11] Xu S Y, Ma Q, Shen H, Fatemi V, Wu S, Chang T R, Chang G, Valdivia A M M, Chan C K, Gibson Q D, Zhou J, Liu Z, Watanabe K, Taniguchi T, Lin H, Cava R J, Fu L, Gedik N and Jarillo-Herrero P 2018 *Nat. Phys.* **14** 900
[12] Qin M S, Zhu P F, Ye X G, Xu W Z, Song Z H, Liang J, Liu K and Liao Z M 2021 *Chin. Phys. Lett.* **38** 017301
[13] Tsirkin S S, Puente P A and Souza I 2018 *Phys. Rev. B* **97** 035158
[14] König E J, Dzero M, Levchenko A and Pesin D A 2019 *Phys. Rev. B* **99** 155404
[15] Son J, Kim K H, Ahn Y H, Lee H W and Lee J 2019 *Phys. Rev. Lett.* **123** 036806
[16] Papaj M and Fu L 2019 *Phys. Rev. Lett.* **123** 216802
[17] See the Supplemental Material for detailed information on the first-principles calculation method, Berry curvature under $C3$ symmetry and antisymmetric characteristic of transverse current using nonequilibrium Green's function method, which includes Refs. [36–41]
[18] Ashton M, Paul J, Sinnott S B and Hennig R G 2017 *Phys. Rev. Lett.* **118** 106101
[19] Mounet N, Gibertini M, Schwaller P, Campi D, Merkys A, Marrazzo A, Sohier T, Castelli I E, Cepellotti A, Pizzi G and Marzari N 2018 *Nat. Nanotechnol.* **13** 246

[20] Haastrup S, Strange M, Pandey M, Deilmann T, Schmidt P S, Hinsche N F, Gjerding M N, Torelli D, Larsen P M, Riis-Jensen A C, Gath J, Jacobsen K W, Jørgen M J, Olsen T and Thygesen K S 2018 *2D Mater.* **5** 042002
[21] Collins J L, Tadich A, Wu W, Gomes L C, Rodrigues J N B, Liu C, Hellerstedt J, Ryu H, Tang S, Mo S K, Adam S, Yang S A, Fuhrer M S and Edmonds M T 2018 *Nature* **564** 390
[22] Hong Y L, Liu Z, Wang L, Zhou T, Ma W, Xu C, Feng S, Chen L, Chen M L, Sun D M, Chen X Q, Cheng H M and Ren W 2020 *Science* **369** 670
[23] Lu A Y, Zhu H, Xiao J, Chuu C P, Han Y, Chiu M H, Cheng C C, Yang C W, Wei K H, Yang Y, Wang Y, Sokaras D, Nordlund D, Yang P, Muller D A, Chou M Y, Zhang X and Li L J 2017 *Nat. Nanotechnol.* **12** 744
[24] Zhang J, Jia S, Kholmanov I, Dong L, Er D, Chen W, Guo H, Jin Z, Shenoy V B, Shi L and Lou J 2017 *ACS Nano* **11** 8192
[25] Bahuguna B P, Saini L K, Tiwari B and Sharma R O 2016 *RSC Adv.* **6** 52920
[26] Weng H, Ranjbar A, Liang Y, Song Z, Khazaei M, Yunoki S, Arai M, Kawazoe Y, Fang Z and Dai X 2015 *Phys. Rev. B* **92** 075436
[27] Reis F, Li G, Dudy L, Bauernfeind M, Glass S, Hanke W, Thomale R, Schäfer J and Claessen R 2017 *Science* **357** 287
[28] Chang K, Liu J, Lin H, Wang N, Zhao K, Zhang A, Jin F, Zhong Y, Hu X, Duan W, Zhang Q, Fu L, Xue Q K, Chen X and Ji S H 2016 *Science* **353** 274
[29] Qian X, Liu J, Fu L and Li J 2014 *Science* **346** 1344
[30] Jia Z Y, Song Y H, Li X B, Ran K, Lu P, Zheng H J, Zhu X Y, Shi Z Q, Sun J, Wen J, Xing D and Li S C 2017 *Phys. Rev. B* **96** 041108(R)
[31] Tang S, Zhang C, Wong D, Pedramrazi Z, Tsai H Z, Jia C, Moritz B, Claassen M, Ryu H, Kahn S, Jiang J, Yan H, Hashimoto M, Lu D, Moore R G, Hwang C C, Hwang C, Hussain Z, Chen Y, Ugeda M M, Liu Z, Xie X, Devereaux T P, Crommie M F, Mo S K and Shen Z X 2017 *Nat. Phys.* **13** 683
[32] Xiao D, Liu G B, Feng W, Xu X and Yao W 2012 *Phys. Rev. Lett.* **108** 196802
[33] Nguyen-Truong H T 2016 *Appl. Phys. Lett.* **108** 172901
[34] Gall D 2016 *J. Appl. Phys.* **119** 085101
[35] Mandal D, Das K and Agarwal A 2020 *Phys. Rev. B* **102** 205414

Supplementary Materials for "Magnus Hall Effect in Two-dimensional Materials"

1. CALCULATION METHODS

The first-principles calculations based on density functional theory (DFT) are performed by using the QUANTUM-ESPRESSO package[1]. Ultrasoft pseudopotentials and general gradient approximation (GGA) according to the Perdew-Burke-Ernzerhof (PBE) functional are used. The energy cutoff of the plane wave (charge density) basis is set to 50 Ry (500 Ry). The DFT Bloch wave functions are projected to maximally localized Wannier functions by Wannier90 code [2, 3]. The Berry curvature is calculated by the WannierTools software package [4]. The spin-orbit coupling is included in all the electronic calculations. The crystal structures are set to make the vertical mirrors or axis be perpendicular to the x direction. All of the band structures are cross-checked by the VASP codes, and the results are consistent with each other.

2. THE BERRY CURVATURE UNDER $\mathcal{C}_3$ SYMMETRY

Every $\mathbf{k}$ point under the $\mathcal{C}_3$ and $\mathcal{T}$ will transform into six points, as shown in Fig. S1. The relationships of velocity and Berry curvature of the six points are listed in Table S1. We can conclude that the $\mathcal{C}_3$ and $\mathcal{T}$ symmetry cannot guarantee the j_y^0 vanishing according to Eq. (2) in the main text.

3. ANTISYMMETRIC CHARACTERISTIC OF TRANSVERSE CURRENT USING GREEN FUNCTION METHOD

We study the transverse current when the vertical mirror or in-plane two-fold symmetries are not perpendicular to the x axis with the non-equilibrium Green's function method[5, 6]. The effective Hamilton with C_{2v} symmetry reads as:

$$H(\mathbf{k}) = Ak^2 + \left(Bk^2 + \delta\right)\sigma_z + v_y k_y \sigma_y + D\sigma_x. \qquad (1)$$

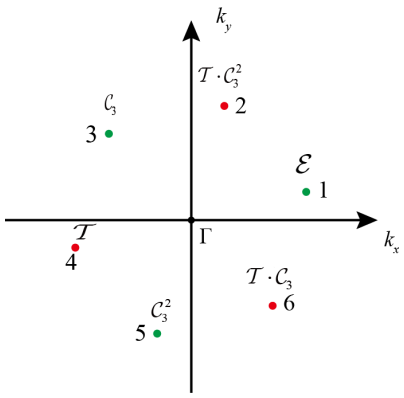

FIG. S1: $\mathbf{k}$ points under the $\mathcal{C}_{3z}$ and $\mathcal{T}$ symmetry. The green and red dots stand for the $\mathbf{k}$ points have the opposite Berry curvature value.

TABLE S1: The relationships of velocity and Berry curvature of the six points in Fig. S1. $\mathcal{E}$ means the identity symmetry.

Point	Operation	Velocity	Ω_z
1	$\mathcal{E}$	(v_x, v_y)	Ω_z
3	$\mathcal{C}_{3z}$	$\left(-\frac{v_x}{2} - \frac{\sqrt{3}v_y}{2}, \frac{\sqrt{3}v_x}{2} - \frac{v_y}{2}\right)$	Ω_z
5	$\mathcal{C}_{3z}^2$	$\left(-\frac{v_x}{2} + \frac{\sqrt{3}v_y}{2}, -\frac{\sqrt{3}v_x}{2} - \frac{v_y}{2}\right)$	Ω_z
2	$\mathcal{T}\cdot\mathcal{C}_{3z}^2$	$\left(\frac{v_x}{2} - \frac{\sqrt{3}v_y}{2}, \frac{\sqrt{3}v_x}{2} + \frac{v_y}{2}\right)$	$-\Omega_z$
4	$\mathcal{T}$	$(-v_x, -v_y)$	$-\Omega_z$
6	$\mathcal{T}\cdot\mathcal{C}_{3z}$	$\left(\frac{v_x}{2} + \frac{\sqrt{3}v_y}{2}, -\frac{\sqrt{3}v_x}{2} + \frac{v_y}{2}\right)$	$-\Omega_z$

where $A = 0$, $B = 1$, $\delta = -0.25$, $v_y = 1.0$ and $D = 0.1$. Then, a voltage drop ΔU is added between the two terminals of the system. The sample size is 80×100, and disorder w=0.2.

The calculated G_{yx} of 0° and 180° with the non-equilibrium Green's function (NEGF) method are shown in Figs. S2 (a) and (b). Because the vertical mirror and in-plane two-fold symmetries are perpendicular to the x axis, only the Magnus Hall part contributes to the transverse current, and G_H are opposite in these two situations. Then, the Hamiltonian in Eq. (1) is rotated counter-clockwise by 45° and 45° + 180°, respectively. When the sample is rotated 45°, the vertical mirror and in-plane two-fold symmetries are not perpendicular to the x axis, the Magnus Hall signals accompany with trivial transverse signals. However, we found that the G_{yx} shows the asymmetry under 45° and 45° + 180°, in Figs. S2 (c) and (d). Because G_y^0 remains invariant, while the G_H is reversed. So the total transverse conductance changes from $G_y^0 + G_H$ to $G_y^0 - G_H$, therefore the antisymmetric part of the total transverse current of these two cases correspond to the Magnus Hall current. The calculated results agree with our symmetry analysis.

4. AFFECT ON LONGITUDINAL ACCELERATION OF ELECTIONS

The built-in electric field is very small, and the wave packet momentum $\mathbf{k}$ does not change substantially under the built-in electric field in the MHE theory [7]. This assumption is reasonable, which can be obtained in the following estimation. The electron velocity $v \sim 10^6$ m/s [8] in conventional metals. If the length of the bottom gate L=100 nm and $\Delta U = 0.1$ eV, we get

$$\Delta k \approx -\frac{1}{\hbar}\frac{\Delta U}{v_x} \approx 0.015 \text{Å}^{-1} \qquad (2)$$

according to Eq. 1 of Ref. [7]. Δk is very small relative to the reciprocal lattice (in the order of 2π Å^{-1}). Correspondingly, the electron velocity $\mathbf{v}$ is basically invariant during the Magnus Hall transport. Besides, the nonequilibrium Green's function method (Landauer-Buttiker simulation) in Ref. [7] and our work do not adopt the assumption that crystal momentum $\mathbf{k}$ and velocity is conserved. However, the results basically match with those using the assumption.

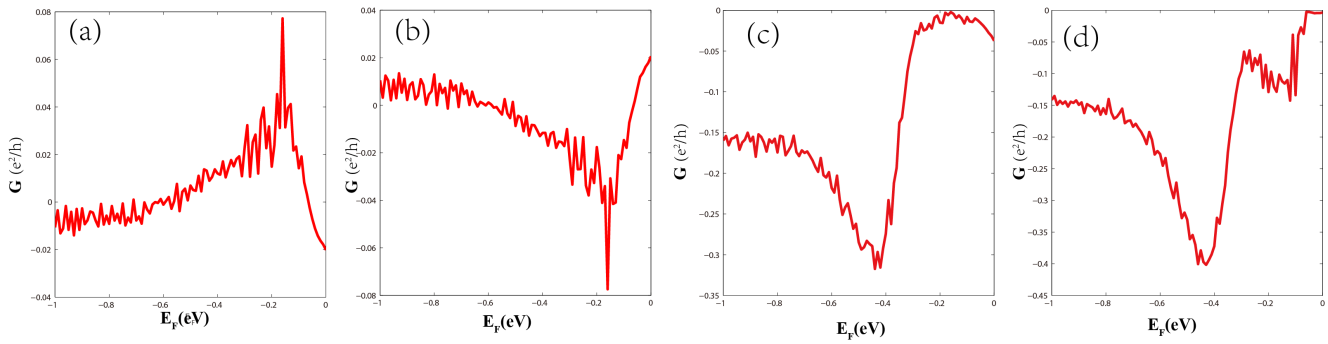

FIG. S2: The transverse conductance when the sample is rotated to (a) 0°, (b) 180°, (c) 45°, and (d) 45° + 180°. The burr is due to the Fabry-Perot resonance in the sample.

If the assumption that crystal momentum conservation breaks down, we think the Magnus Hall can also exist. Eq. 2 of Ref. [7] will be

$$\Delta y_A = -\int_0^t \frac{\Omega_z(\mathbf{k})}{\hbar}\frac{\partial U}{\partial x}dt = -\int_0^L \frac{\partial k_x}{\partial \varepsilon(\mathbf{k})}\Omega_z(\mathbf{k})\frac{\partial U}{\partial x}dx \quad (3)$$

where t is the transit time through the electric field region. During this time, crystal moment changes, *i.e.*, is the function of time t. This equation will be very complicated, cannot have an analytical solution. In this case, we have to adopt the nonequilibrium Green s function method to study this, while it is beyond the scope of our study.

[1] P. Giannozzi, S. Baroni, N. Bonini, M. Calandra, R. Car, C. Cavazzoni, D. Ceresoli, G. L. Chiarotti, M. Cococcioni, I. Dabo, A. D. Corso, S. d. Gironcoli, S. Fabris, G. Fratesi, R. Gebauer, U. Gerstmann, C. Gougoussis, A. Kokalj, M. Lazzeri, L. Martin-Samos, N. Marzari, F. Mauri, R. Mazzarello, S. Paolini, A. Pasquarello, L. Paulatto, C. Sbraccia, S. Scandolo, G. Sclauzero, A. P. Seitsonen, A. Smogunov, P. Umari, and R. M. Wentzcovitch, J. Phys.: Condens. Matter. **21**, 395502 (2009).

[2] A. A. Mostofi, J. R. Yates, Y.-S. Lee, I. Souza, D. Vanderbilt, and N. Marzari, Comput. Phys. Commun. **178**, 685 (2008).

[3] A. A. Mostofi, J. R. Yates, G. Pizzi, Y.-S. Lee, I. Souza, D. Vanderbilt, and N. Marzari, Comput. Phys. Commun. **185**, 2309 (2014).

[4] Q. Wu, S. Zhang, H.-F. Song, M. Troyer, and A. A. Soluyanov, Comput. Phys. Commun. **224**, 405 (2018).

[5] Q. Yan, Y.-F. Zhou, and Q.-F. Sun, Chin. Phys. B. **29**, 097401 (2020).

[6] Y.-H. Li, J. Liu, J. Song, H. Jiang, Q.-F. Sun, and X. Xie, Science China Physics, Mechanics & Astronomy **61**, 97411 (2018).

[7] M. Papaj and L. Fu, Phys. Rev. Lett. **123**, 216802 (2019).

[8] D. Gall, J. Appl. Phys. **119**, 085101 (2016).